Manuscript submitted to Journal of Geophysical Research: Solid Earth

Supporting Information for

Upper-mantle anisotropy in the southeastern margin of the Tibetan Plateau revealed by fullwave SKS splitting intensity tomography

Yi Lin[1,2] and Li Zhao[1,3*]

[1] *School of Earth and Space Sciences, Peking University, Beijing 100871, China.*

[2] *Key Laboratory of Earth Exploration and Information Techniques of the China Ministry of Education, Chengdu University of Technology, Chengdu 610059, China.*

[3] *Hebei Hongshan National Geophysical Observatory, Peking University, Beijing 100871, China.*

* Corresponding author: Li Zhao (lizhaopku@pku.edu.cn)

This Supporting Information contains 8 Supplementary Figures S1-S8.

Figure S1: Resolution test results at different depths for the azimuth of symmetry axis using 1º x 1º checkerboard and different damping factors.

Figure S2: Resolution test results at different depths for anisotropy strength using 1º x 1º checkerboard and different damping factors.

Figure S3: Resolution test results at different depths for the azimuth of symmetry axis using 1.5º x 1.5º checkerboard and different damping factors.

Figure S4: Resolution test results at different depths for anisotropy strength using 1.5º x 1.5º checkerboard and different damping factors.

Figure S5: Resolution tests for the azimuth of symmetry axis using a 2-layer input model and different damping factors.

Figure S6: Resolution tests for anisotropy strength using a 2-layer input model and different damping factors.

Figure S7: Resolution tests for the azimuth of symmetry axis using a 4-layer input model and different damping factors.

Figure S8: Resolution tests for anisotropy strength using a 4-layer input model and different damping factors.

Supplementary Figures

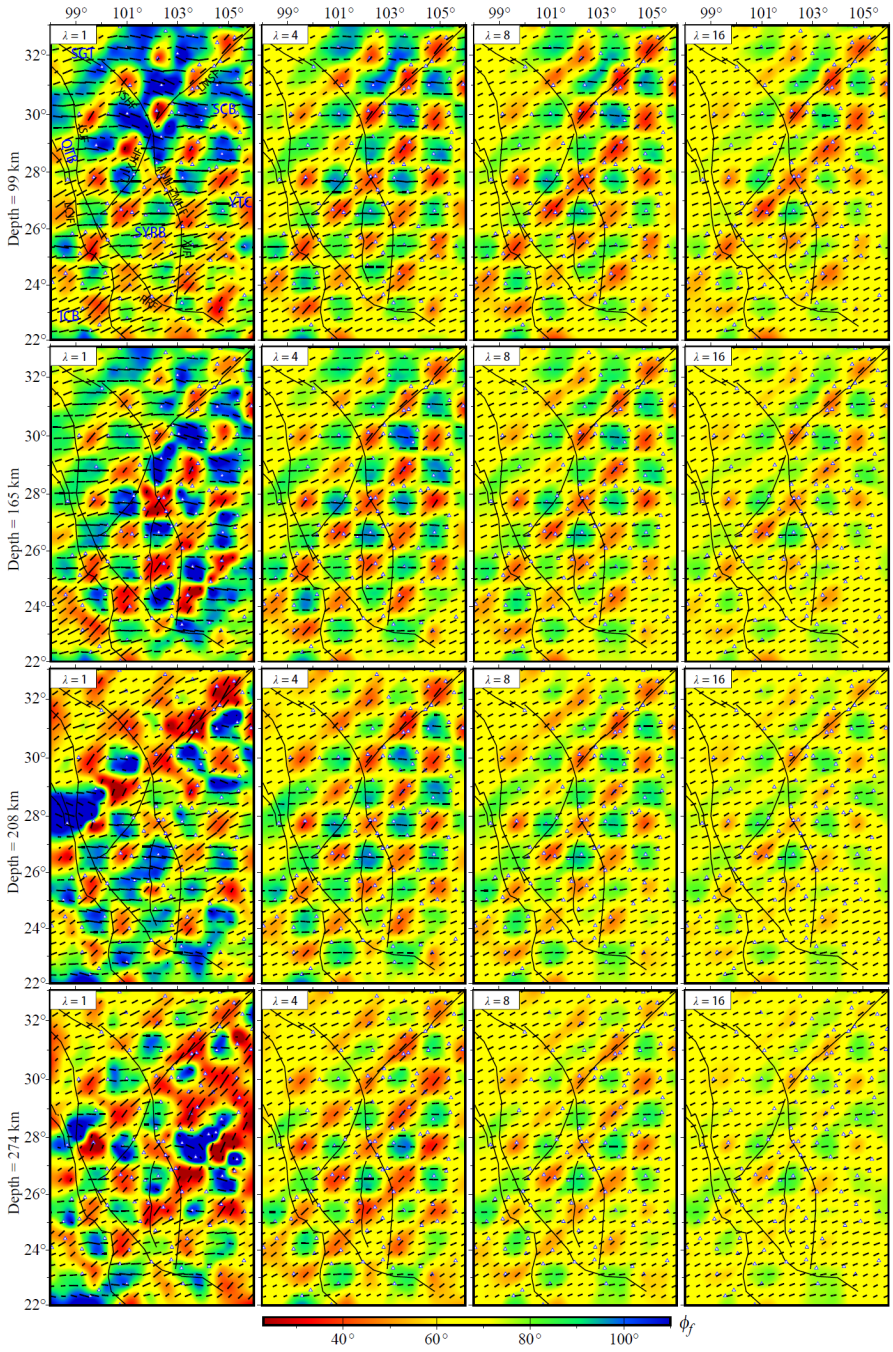

Figure S1. Resolution tests for the azimuth of symmetry axis using 1º x 1º checkerboard. The input model (top-left panel of Figure 8) has horizontally alternating azimuthal angles of fast axes $\phi_f = 90^\circ$ and $\phi_f = 45^\circ$ shown by both the color and the directions of the line segments, and a fixed anisotropy strength $\gamma = 4\%$ represented by the lengths of the line segments. Shown here are recovered models using different damping factors (left to right) at different depths (top to bottom).

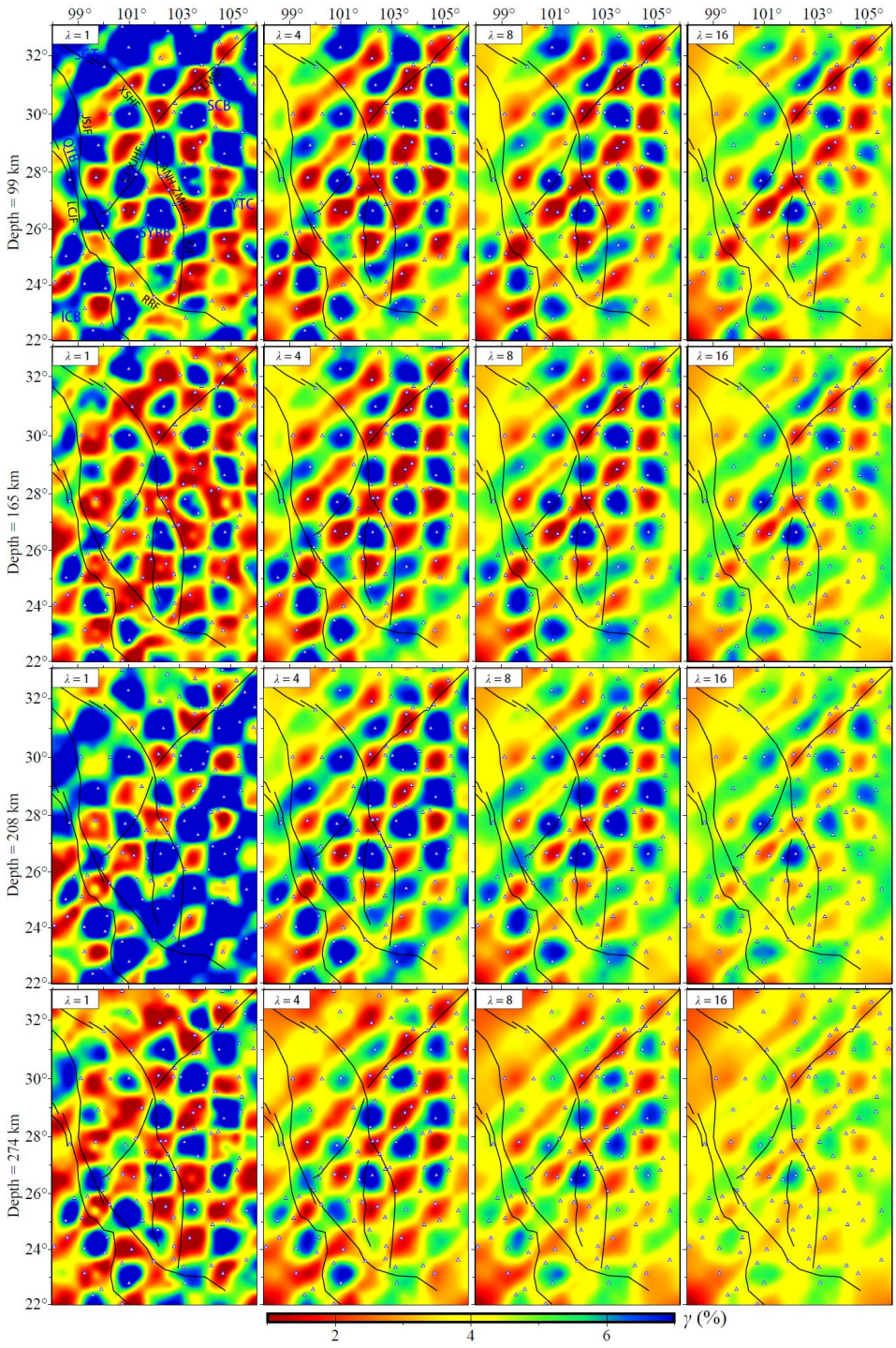

Figure S2. Resolution tests for anisotropy strength using 1° x 1° checkerboard. The input model (top-left panel of Figure 8) has horizontally alternating anisotropy strengths shown by the colors representing perturbations of $\delta\gamma = \pm 0.03$ relative to a background anisotropy strength of $\gamma = 0.04$ and a fixed azimuthal angle of symmetry axis $\phi_f = 22.5^{\circ}$. Shown here are recovered models using different damping factors (left to right) at different depths (top to bottom).

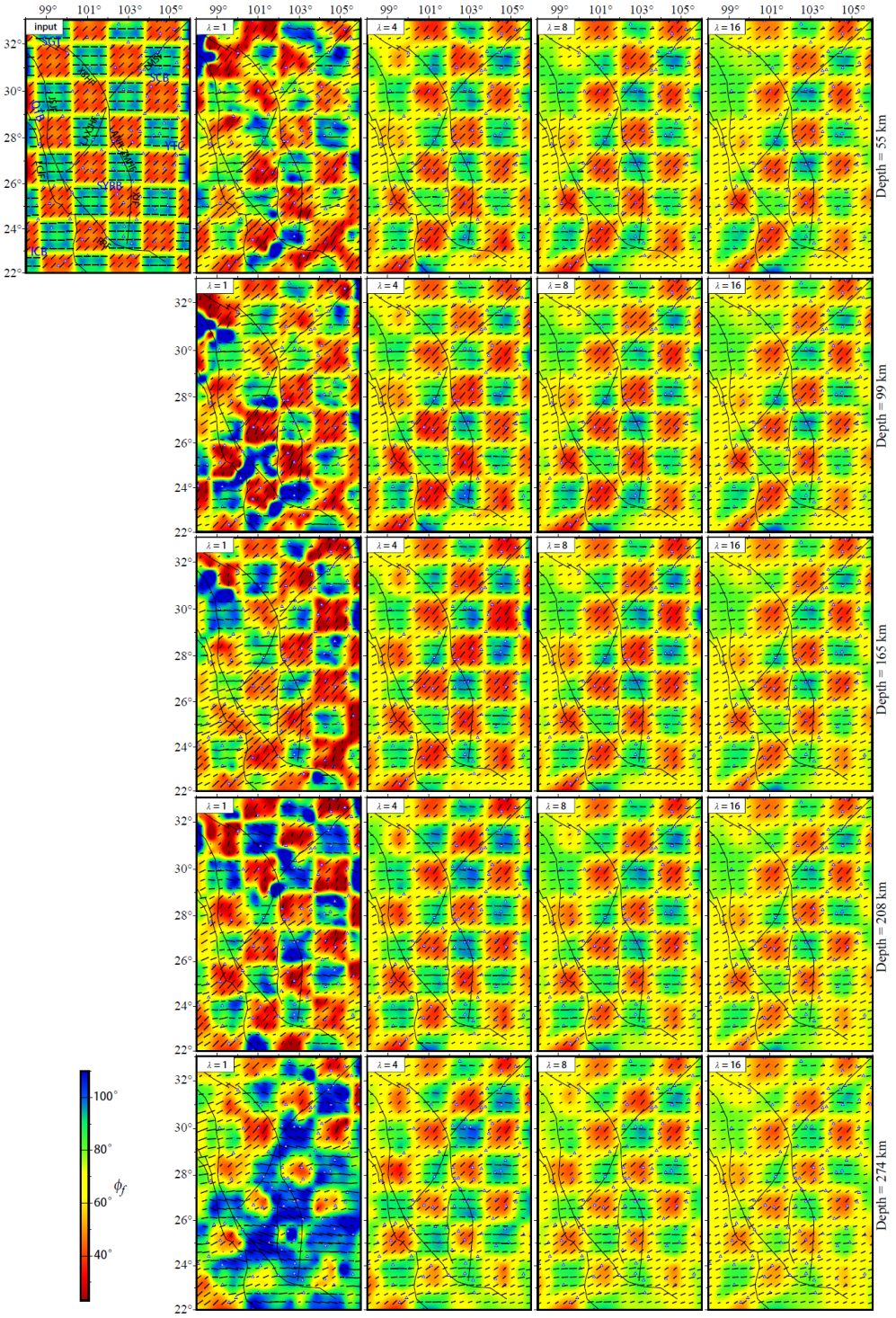

Figure S3. Resolution tests for the azimuth of symmetry axis using 1.5º x 1.5º checkerboard. The input model (top-left panel) has horizontally alternating azimuthal angles of fast axes $\phi_f = 90^\circ$ and $\phi_f = 45^\circ$ shown by both the color and the directions of the line segments, and a fixed anisotropy strength $\gamma = 4\%$ represented by the lengths of the line segments. The rest of the panels show recovered models using different damping factors (left to right) at different depths (top to bottom).

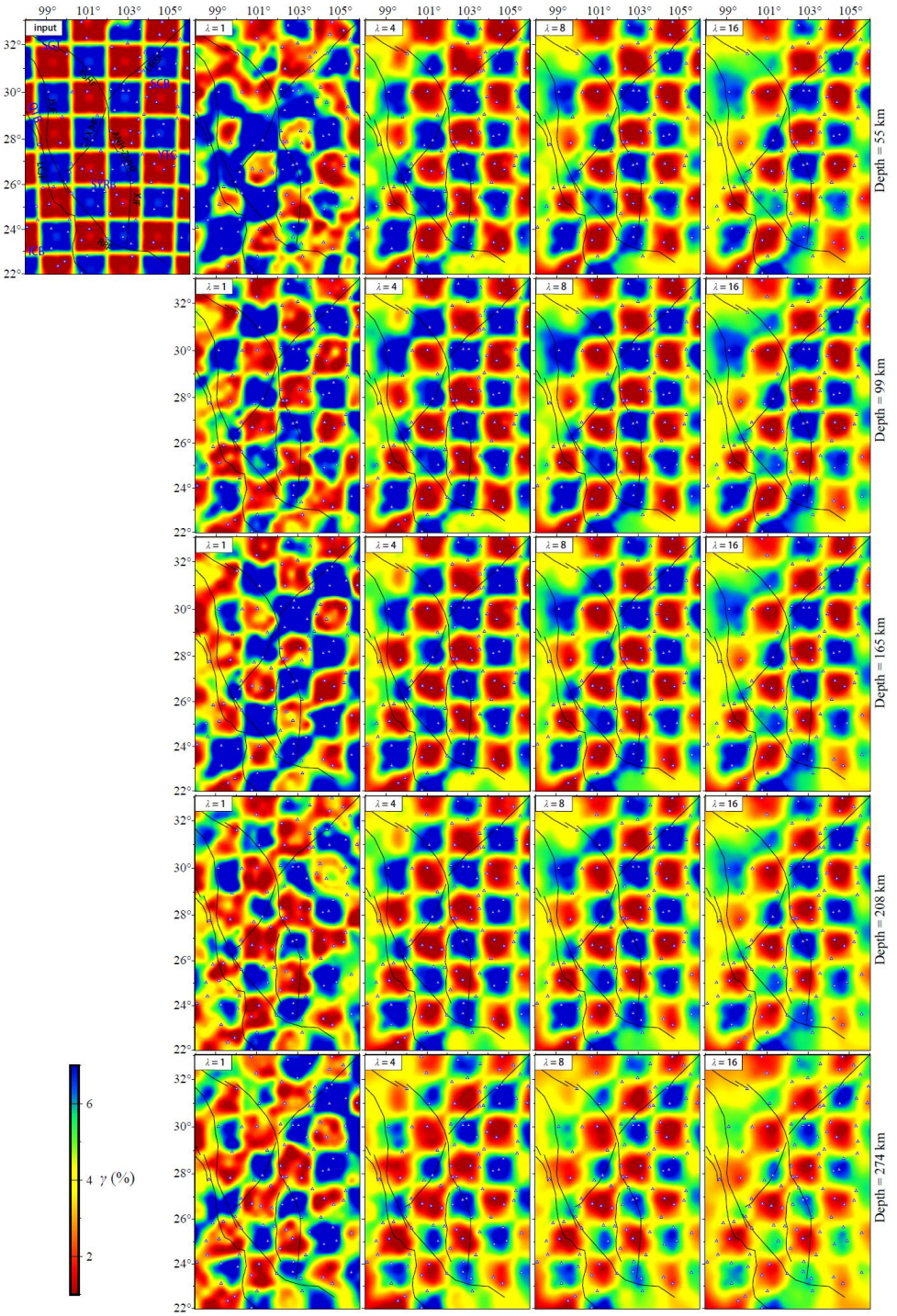

Figure S4. Resolution tests for anisotropy strength using 1.5º x 1.5º checkerboard. The input model (top-left panel) has horizontally alternating anisotropy strengths shown by the colors representing perturbations of $\delta\gamma = \pm 0.03$ relative to a background anisotropy strength of $\gamma = 0.04$ and a fixed azimuthal angle of symmetry axis $\phi_f = 22.5^{\circ}$. The rest of the panels show recovered models using different damping factors (left to right) at different depths (top to bottom).

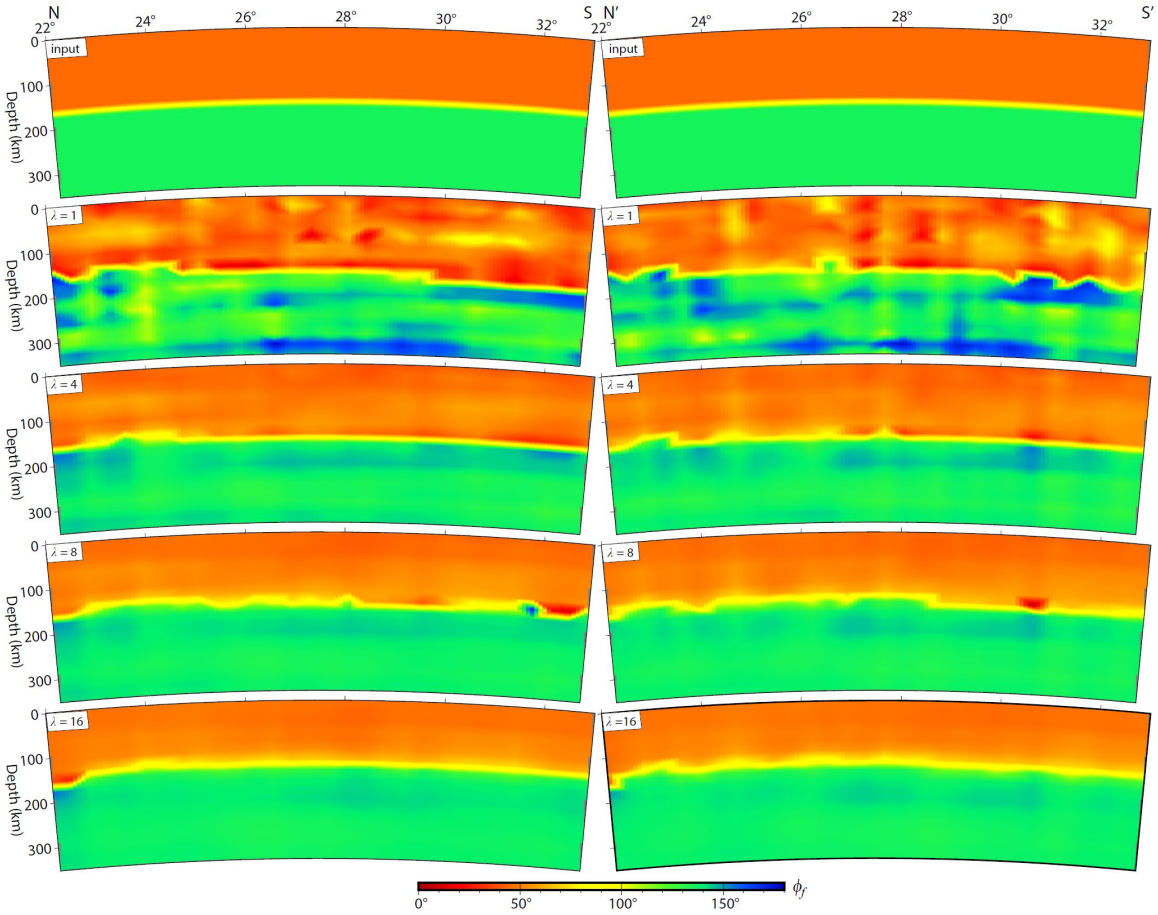

Figure S5. Resolution tests for an input model with 2 layers of different azimuthal angles of symmetry axes $\phi_f = 45^\circ$ and $\phi_f = 135^\circ$ but a fixed anisotropy strength of $\gamma = 4\%$. Shown here are the input models (top two panels) along the NS and N'S' cross-sections (see top-left panel in Figure 8 for the locations of the cross-sections) and recovered models for different damping factors λ (lower panels).

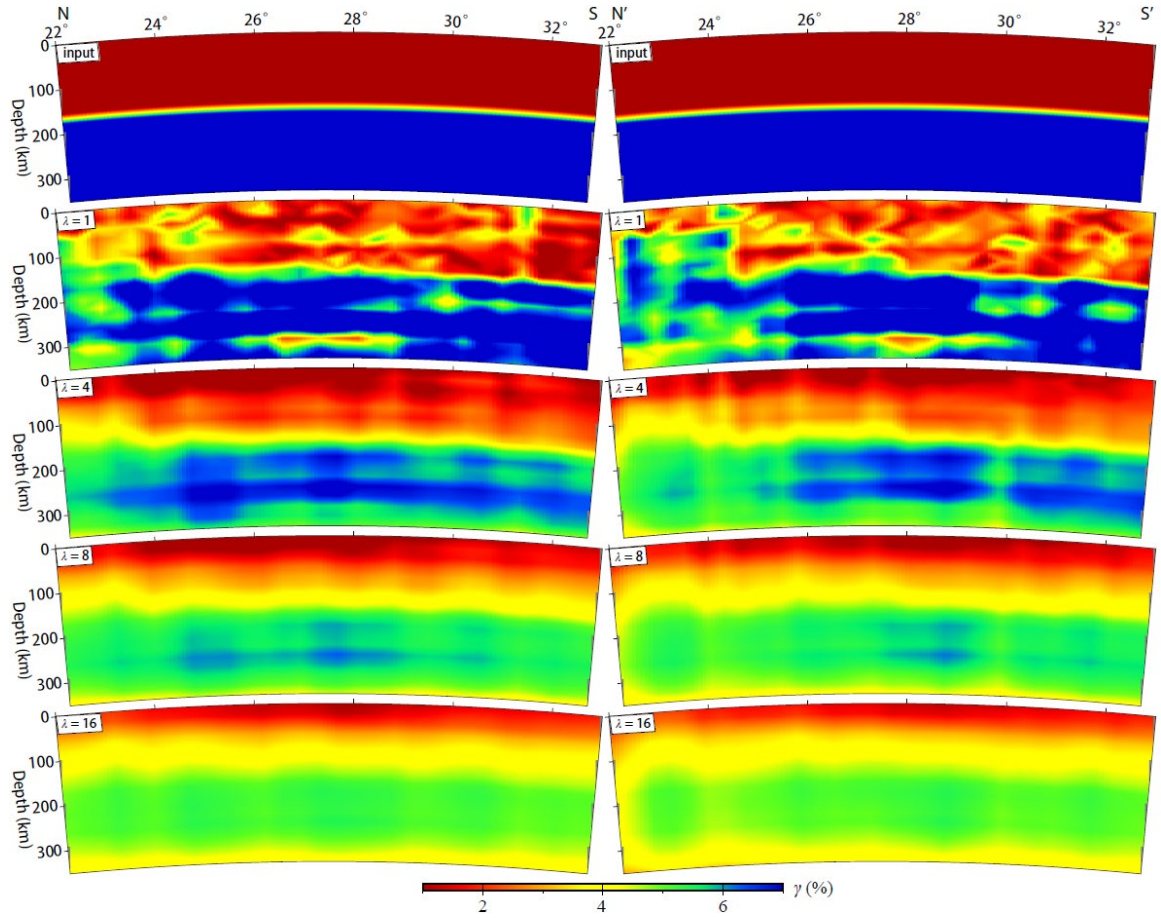

Figure S6. Resolution tests for an input model with 2 layers of different anisotropy strengths shown by the colors representing perturbations of $\delta\gamma = \pm 0.03$ relative to a background anisotropy strength of $\gamma = 0.04$ and a fixed azimuthal angle of symmetry axis $\phi_f = 22.5^{\circ}$. Shown here are the input models (top two panels) along the NS and N'S' cross-sections (see top-left panel in Figure 8 for the locations of the cross-sections) and recovered models for different damping factors λ (lower panels).

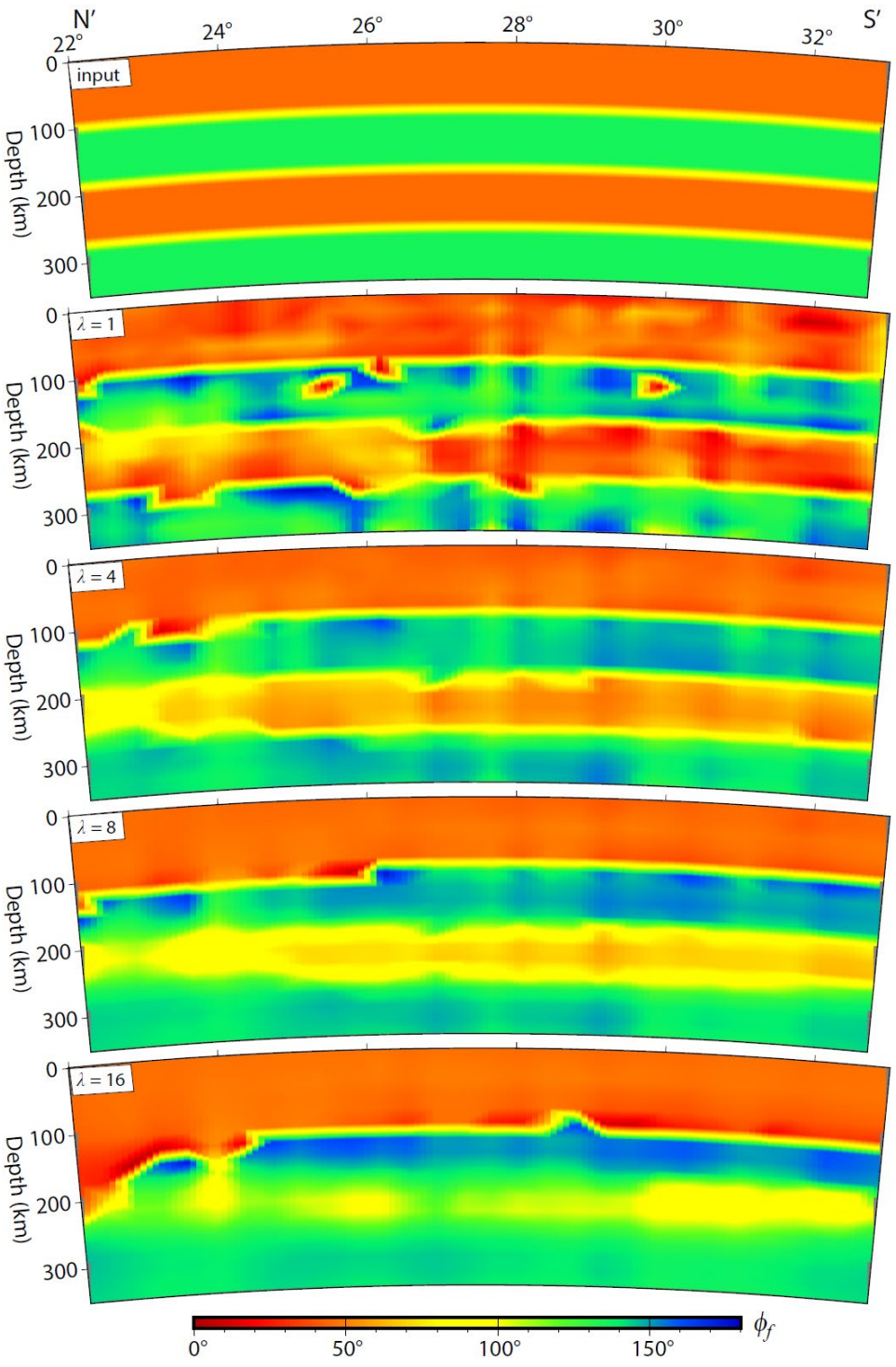

Figure S7. Resolution tests for an input model with 4 layers of alternating azimuthal angles of symmetry axes $\phi_f = 45^\circ$ and $\phi_f = 135^\circ$ but a fixed anisotropy strength of $\gamma = 4\%$. Shown here are the input model (top panel) along the N'S' cross-section (see top-left panel in Figure 8 for the location of the cross-section) and recovered models for different damping factors λ (lower panels).

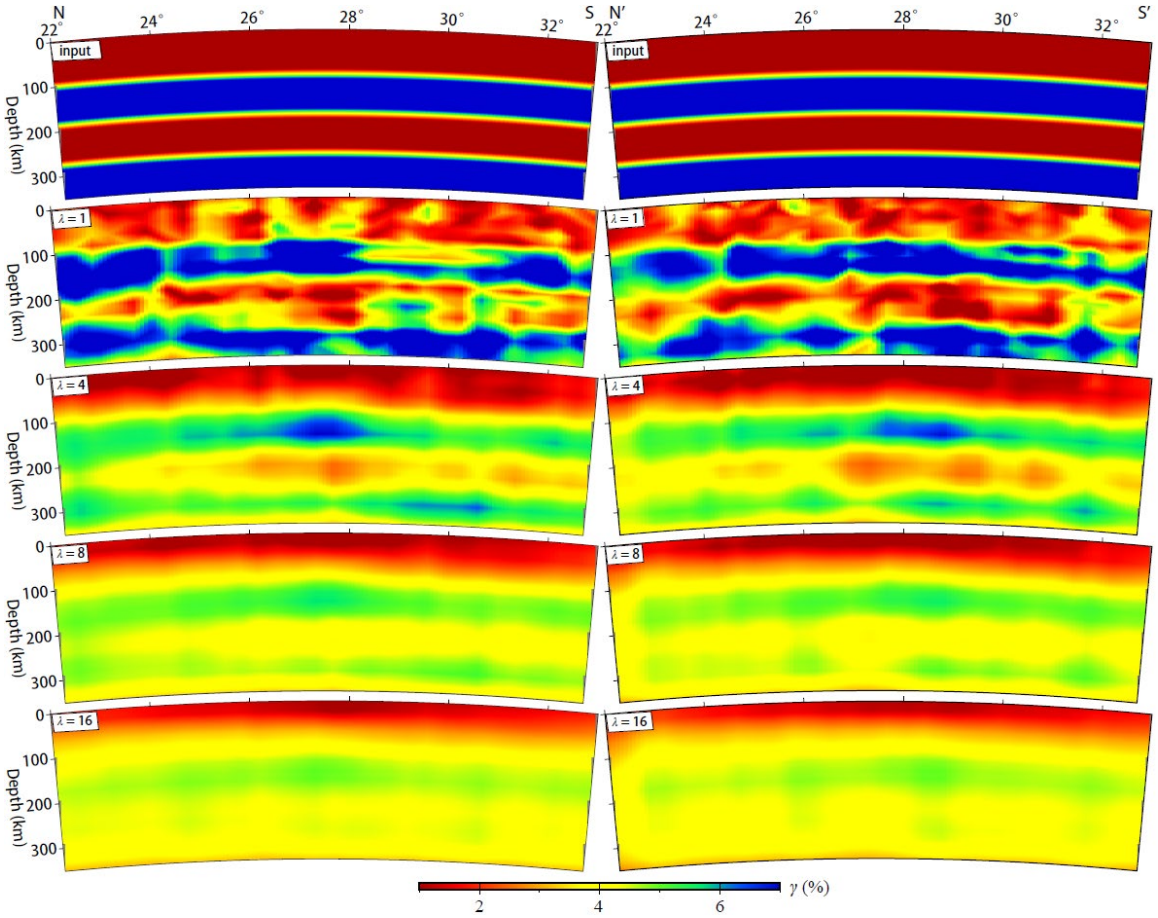

Figure S8. Resolution tests for an input model with 4 layers of alternating anisotropy strengths shown by the colors representing perturbations of $\delta\gamma = \pm 0.03$ relative to a background anisotropy strength of $\gamma = 0.04$ and a fixed azimuthal angle of symmetry axis $\phi_f = 22.5^{\circ}$. Shown here are the input models (top two panels) along the NS and N'S' cross-sections (see top-left panel in Figure 8 for the locations of the cross-sections) and recovered models for different damping factors λ (lower panels).